Rapid field application of hydraulic tomography for resolving aquifer heterogeneity in unconsolidated sediments

R. Brauchler, ¹ R. Hu, ² L. Hu, ² S. Jiménez, ¹ P. Bayer, ¹ P. Dietrich, ^{3,4} and T. Ptak ² Received 17 July 2012; revised 4 March 2013; accepted 4 March 2013; published 23 April 2013.

[1] A new framework is introduced for hydraulic tomography application and validation in the field. Our motivation is the need for methods that are both efficient and expressive for resolving the spatial distribution of heterogeneous hydraulic properties in aquifers. The presented strategy involves time-efficient field experiments and a computationally efficient inversion scheme. By exploiting the early travel time diagnostics of the hydraulic pressure pulses recorded during tomographic cross-well tests, and new application of attenuation inversion, only short-term pumping tests are required. Many of these can be conducted in one day. The procedure is developed by a numerical experiment with a highly heterogeneous aquifer analogue and then applied to a field case with a shallow, unconsolidated sedimentary aquifer, the Stegemühle site in Germany. It is demonstrated that the performance of a suite of tomographic short-term pumping tests, data processing and inversion for the reconstruction of heterogeneous diffusivity and specific storage distribution is possible within one day. Additionally, direct-push injection logging is performed at the field site, and the obtained field data is utilized for successful validation of the hydraulic tomograms. We also compare both methods with respect to the necessary requirements, time demand in the field and complexity of interpretation.

Citation: Brauchler, R., R. Hu, L. Hu, S. Jiménez, P. Bayer, P. Dietrich, and T. Ptak (2013), Rapid field application of hydraulic tomography for resolving aquifer heterogeneity in unconsolidated sediments, *Water Resour. Res.*, 49, 2013–2024, doi:10.1002/wrcr.20181.

1. Introduction

- [2] Hydraulic tomography and direct-push (DP) methods were identified as the next generation of hydraulic characterization technologies [Butler, 2005]. Hydraulic tomography involves the combined interpretation of multiple crosswell hydraulic tests. The recorded hydraulic pulses are inverted to characterize the hydraulic conductivity (K) and specific storage (S_s) distributions with a high resolution and accuracy. DP can also serve this purpose, as it allows for low-cost vertical profiling of K at several nearby positions in a shallow aquifer. Since 2005, both methods were further developed and tested at different field sites.
- [3] The centerpiece of DP profiling is the probe, which is attached to a steel pipe string. It is advanced into the ground by the weight of the DP unit, or, if probe design allows, depth of penetration can be augmented by application of a hydraulic percussion hammer. *Liu et al.* [2012] give a comprehensive overview of different DP probes.

They distinguish between probes for absolute and relative K-profiling.

- [4] Absolute K-profiling is performed with the directpush permeameter (DPP), which consists of a probe with a short screen and two pressure transducers attached to the probe surface. After the probe is pushed to the target depth, a short hydraulic test is performed by injecting water through the screen and recording the pressure response at the attached pressure transducers, while the flow is controlled at the surface. A complete test series at one depth level can be performed within 15 min. The DPP probe was proposed and successfully tested at the well-documented Geohydrologic Experimental and Monitoring Site [e.g., Butler, 2005] in Lawrence, Kansas, and at the Nauen site located 40 km west of Berlin, Germany [Yaramanci et al., 2002]. They recorded several K-profiles and validated them by multilevel slug tests and by information obtained from core samples.
- [5] Relative K-profiling is performed with the direct-push injection logger (DPIL), which consists of a probe with a short screen for the injection of water. Pressure and flow are recorded and regulated at the surface using a pressure transducer and a flow controller. Dietrich et al. [2008] proposed a DPIL-probe, which can be used only in a discontinuous mode. This means that the probe advancement has to be stopped at each test interval (depth level). They reconstructed a relative K-profile over a depth of 18 m consisting of 35 measurement points in a fine- to mediumgrained sand aquifer. The profile was obtained within 3 h and validated by core data and slug tests. An alternative DPIL probe, which allows for continuous profiling with a

©2013. American Geophysical Union. All Rights Reserved. 0043-1397/13/10.1002/wrcr.20181

¹Department of Earth Sciences, ETH Zurich, Zurich, Switzerland.

²Geoscientific Centre, University of Göttingen, Göttingen, Germany.

³Helmholtz Centre for Environmental Research (UFZ), Department Monitoring and Exploration Technologies, Leipzig, Germany.

⁴Center of Applied Geoscience, University of Tübingen, Tübingen, Germany.

Corresponding author: R. Brauchler, Department of Earth Sciences, ETH Zurich, Sonneggstrasse 5, Zurich CH-8092, Switzerland. (ralf.brauchler@erdw.ethz.ch)

vertical resolution of 0.015 m was proposed by *McCall et al.* [2009]. This DPIL probe was tested within a sand and gravel aquifer, where several 30 m deep relative *K*-profiles with a vertical resolution of 0.015 m and an advancement rate of 0.02 m/s could be recorded.

- [6] Liu et al. [2009] proposed a new type of probe, which combines the advantages of both the DPIL probe designed for continuous K-profiling and the DPP probe designed for absolute K-profiling. The variant is called "high-resolution K probe" (HRK) and it facilitates sampling of a 10 m profile with a vertical resolution of 0.015 m in less than 30 min. Bohling et al. [2012] applied these hydraulic DP tools to obtain several profiles from the heavily studied MAcro Dispersion Experiment (MADE) site [Boggs et al., 1992] to characterize detailed K-variations at the site. The data are compared with those from the flowmeter profiles that have served as the primary basis for characterizing the heterogeneous aquifer at the site [Rehfeldt et al., 1992]. Overall, the patterns of variation acquired by DP are quite similar to those in the flowmeter data.
- [7] Similar to the rapid development of DP profiling, hydraulic tomography has substantially evolved. Since 2005, several new and improved inversion schemes have been introduced, and the number of hydraulic tomography field studies is continuously increasing. This history documents the transition of hydraulic tomography as theoretic concept that is approved for characterizing synthetic "digital" aquifers to a robust field method to reconstruct hydraulic properties of real aquifers. In addition to K-fields, spatial diffusivity and/or S_S -distributions can be obtained.
- [8] Bohling et al. [2007] proposed a field assessment of hydraulic tomography in unconsolidated sediments utilizing the steady shape flow regime [Wenzel, 1942]. The latter enables evaluation of transient data with the computational efficiency of a steady state model. They reconstructed the spatial K-distribution assuming a given structure of homogeneous horizontally arranged layers that are persistent within the entire model domain. The reconstructions were validated by tracer and DPP tests. For the technical field implementation, the continuous multichannel tubing (CMT) system [Einarson and Cherry, 2002] was applied. This allowed for recording of pressure response at seven different depth levels without using multipacker systems in the observation wells.
- [9] Straface et al. [2007] published the first field hydraulic tomography application that exploits the potential of geostatistically based inversion. The applied procedure relies on the sequential successive linear estimator (SSLE), as proposed by Zhu and Yeh [2005]. The SSLE inversion scheme successively includes the transient head data from different pumping tests, such that the size of the covariance matrix is small and the calculation demand can be reduced. To account for the nonuniqueness issue the hydraulic parameter field is treated as an outcome of a stochastic spatial process, whereby the mean parameter distribution is reconstructed by matching the observations from the pumping test responses. Straface et al. [2007] used this inversion scheme for depth integrated reconstruction of hydraulic conductivity and specific storage fields. However, the reconstructed hydraulic conductivity and specific storage tomograms showed no correlation among each other, which is expected in natural sedimentary aquifers [e.g., Bayer

- et al., 2011], and no additional field data were provided to support the tomograms. Meanwhile, SSLE-based inversions have successfully been applied in other studies as well. Berg and Illman [2011] performed a three-dimensional (3-D) transient hydraulic tomographic field assessment in highly heterogeneous till and glaciofluvial material. The database of their hydraulic tomographic investigations comprises four pumping and up to 41 observation intervals with a pumping time between 6.5 and 24 h. The large number of observation intervals was realized by utilizing a CMT system. The reconstructed 3-D hydraulic conductivity and storage tomograms were validated by a high number of permeameter data.
- [10] A large scale field assessment (>500 m) was performed by Illman et al. [2009]. They analyzed two large-scale cross-hole pumping tests in a granite aguifer to compute hydraulic conductivity and storage tomograms. The reconstructions show several distinct zones characterized by high-hydraulic conductivity and low-specific storage values that are continuous over hundreds of meters. The authors interpreted these features as fault zones. *Huang* et al. [2011] presented a field study of steady state hydraulic tomography in unconsolidated sediments based on 110 pressure response curves, whereby each pumping test was performed for at least 72 h to reach steady state flow conditions. For the inversion, they used the scheme of Xiang et al. [2009], which is an improved SSLE allowing for the simultaneous inversion of all drawdown curves. The reconstructed tomograms displayed a depth integrated distribution of hydraulic conductivity and storage, and they were validated by matching the drawdown of pressure response curves that were not used for the inversion. Li et al. [2008] also employed a geostatistical approach to jointly invert data from steady state pumping tests and flowmeter measurements to estimate hydraulic conductivity in three dimensions. The pumping tests were performed in 29 fully screened wells and it took about 2 h to reach steady state conditions.
- [11] The first hydraulic tomographic field study in an unconfined aquifer was presented by *Cardiff et al.* [2009]. The steady state inversion is based on nine dipole pumping tests performed in unconsolidated gravel and sand sediments. The tests were designed in a way that a full set of drawdown and recovery data can be collected in one working day. For the reconstruction of the depth integrated hydraulic conductivity field data, the Bayesian geostatistical inversion method proposed by *Kitanidis* [1995] was utilized.
- [12] An alternative inversion approach is based on a transformation of the transient groundwater flow equation into the eikonal equation, using an asymptotic approach [Virieux et al., 1994]. The eikonal equation can be solved with less computational effort using ray tracing techniques, i.e., calculation of trajectories, or particle tracking methods that allow for the calculation of transient pressure propagation along trajectories [Vasco et al., 2000]. He et al. [2006] further developed the approach by Vasco et al. [2000] through matching the amplitudes in addition to travel time. For the inversion, they used an iterative sparse matrix solver [Paige and Saunders, 1982]. In their application, two pumping tests were performed in naturally fractured limestone. They showed that the reconstruction of a twodimensional (2-D) permeability tomogram enables one to image an orthogonal fracture pattern, which could be validated by seismic tomographic measurements.

- [13] Brauchler et al. [2010] applied a similar travel time based inversion scheme to cross-well interference slug tests at the Stegemühle site in Germany which consists of a shallow, 2 m thick sand and gravel aquifer overlain by a confining clay layer with a thickness of 2–3 m. They inverted the pressure response of 196 cross-well interference slug tests performed between five wells. Based on a travel time inversion scheme proposed by Brauchler et al. [2003], they reconstructed the 2-D diffusivity distribution of the aquifer. Brauchler et al. [2011] further developed the inversion approach and inverted cross-well interference slug tests with a travel time and attenuation based inversion scheme. They obtained the diffusivity and specific storage distribution between the wells in two and three dimensions.
- [14] The hydraulic tomographic field applications so far have shown that the method is suitable for mapping hydraulic subsurface features and for estimating the hydraulic parameters hydraulic conductivity and storage in 2-D and 3-D. However, obtaining a high-spatial resolution by hydraulic tomographic investigation is still accompanied by relative complex analysis [Bohling et al., 2002], partly high-computational costs, and relative long pumping times.
- [15] In this paper, we propose a field strategy for hydraulic tomography that can be (a) analyzed and (b) performed with a similar speed as DP profiling. (a) Therefore, we further developed the computationally efficient travel time and attenuation based inverse scheme proposed by Brauchler et al. [2011]. The inverse scheme allows for the inversion of Dirac signals and was successfully applied to the inversion of cross-well interference slug tests. In this work we further develop the inverse scheme and adapt it to the requirements of Heaviside signals and apply it to the inversion of shortterm pumping tests. Beyond this, we introduce the concept of null space energy maps for the validation of the hydraulic tomograms, which was originally developed for geophysical ray tomography. The further developed inverse scheme is tested numerically with data from a hydraulic tomography analogue outcrop study. (b) The field implementation is realized in a way that a suite of tomographic measurements can be recorded in 1 day. Therefore, we limit the pumping time to 300 s, which permits us to record 30 transient pressure response curves between a 2" well (pumping well) and a CMT (observation well) in a few hours. The reconstructed tomograms are compared and evaluated by means of four DPIL logs performed between the pumping and the observation well.

2. Field Data Processing and Inversion Methodology

[16] In the following, we introduce the fundamental concept of travel time based inversion as shown in detail by *Brauchler et al.* [2011], and discuss the requirements for field data processing. Then, a novel adaptation of the attenuation based inversion scheme to the inversion of pumping tests signals is proposed. The methodology is first applied to a numerical example. The gained experience is exploited for a field demonstration and validation with DPIL.

2.1. Travel Time Inversion of Pumping Tests Data

[17] The proposed travel time inversion is based on the work of *Vasco et al.* [2000]. They developed an inversion

scheme based on the transformation of the groundwater flow equation into the eikonal equation [Virieux et al., 1994], which can be solved with ray tracing or particle tracking methods in a computationally efficient way. The keystone of the procedure is the following line integral proposed by Vasco et al. [2000]:

$$h_h(r, t_{\alpha,h}) = \alpha_h h_{\text{max}}; \qquad 0 < \alpha_h < 1 \tag{1}$$

where $t_{\rm peak}$ is defined as the source-to-observation-point travel time of the peak of a transient pressure curve, resulting from a Dirac signal generated at point x_1 (source), traveling along the propagation path s, and recorded at point x_2 (observation point). D is the diffusivity. In a homogeneous media equation (1) can be expressed as follows [Vasco et al., 2000]:

$$t_{\text{peak}} = \frac{S_S r^2}{6K},\tag{2}$$

where S_s is the specific storage, r is the distance between the source and the observation point, and K the hydraulic conductivity. Equation (1) is only valid for an impulsive type source (Dirac source) and was successfully applied to invert travel times derived from cross-well interference slug tests by $Brauchler\ et\ al.\ [2010]$. $Vasco\ et\ al.\ [2000]$ showed that the pressure response of a pumping test signal, usually described with a Heaviside function, can be analyzed as a response to an impulsive (Dirac delta) type source by considering the time-derivative of head data. This differentiation when applied to field data comprises three steps:

- [18] (1) Wavelet de-noising [e.g., *Xiang et al.*, 2009] is utilized to smooth the transient head data.
- [19] (2) A polynomial regression is applied to the smoothed transient head data.
- [20] (3) The first derivative of the polynomial fit is estimated. The three steps are depicted in Figure 1a.

2.2. Travel Time Diagnostics

[21] For travel time inversion, we use an early travel time diagnostic rather than the peak travel time. Brauchler et al. [2007] defined the travel time diagnostic as "the time of occurrence of a certain feature of the transient pressure pulse". The t-10% diagnostic in this study is the time at which the time derivative of the pressure pulse rises to 10% of its ultimate peak (Figure 1a). In this study, we decided to use the t-10% diagnostic for the numerical example and the t-50% diagnostic for the field example. The choice of the travel time diagnostics is a compromise between data quality (early time noise) and the findings of Cheng et al. [2009] that early travel times are better suited to resolve the diffusivity distribution of an aquifer. Figure 1 shows that the travel time diagnostic t_{peak} can be determined with a high level of confidence. In order to determine the uncertainty associated with the choice of the 50% travel time diagnostics, used in the field example, we performed a Monte Carlo analysis. The filtered signal of the pressure response curve displayed in Figure 1 was fitted with a Gaussian function consisting of 4 terms and 12 coefficients. For 2800 fits, the travel time diagnostic t-50% and t_{peak} were calculated. The 2800 calculated travel time diagnostics t-50%

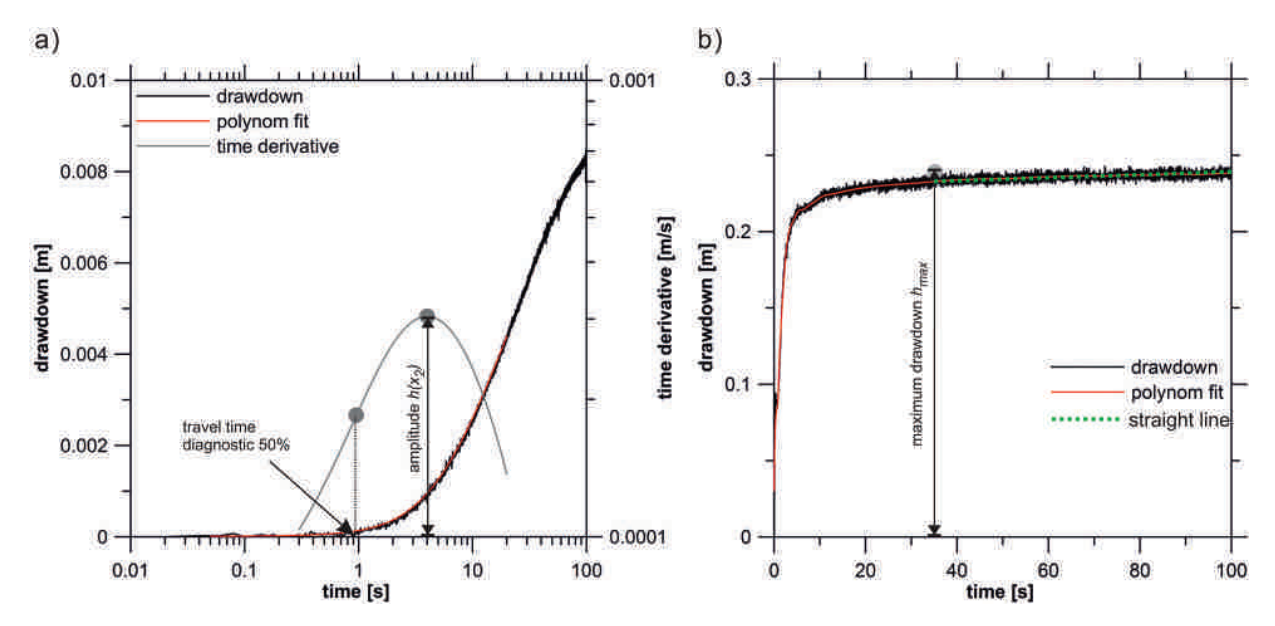


Figure 1. Field data processing. (a) Processing of the pressure response recorded at the observation interval. (b) Processing of the pressure response recorded at the pumping interval.

are characterized by a mean of 1.16 s and an associated standard deviation of 0.076 s. The comparison with the 2800 calculated travel time diagnostics t-peak characterized by a mean value of 4.03 s and an associated standard deviation of 0.84 indicates that the travel time diagnostic t-50% can be determined with a comparable accuracy as the travel time diagnostic $t_{\rm peak}$. In Figure 2, additionally, the statistical

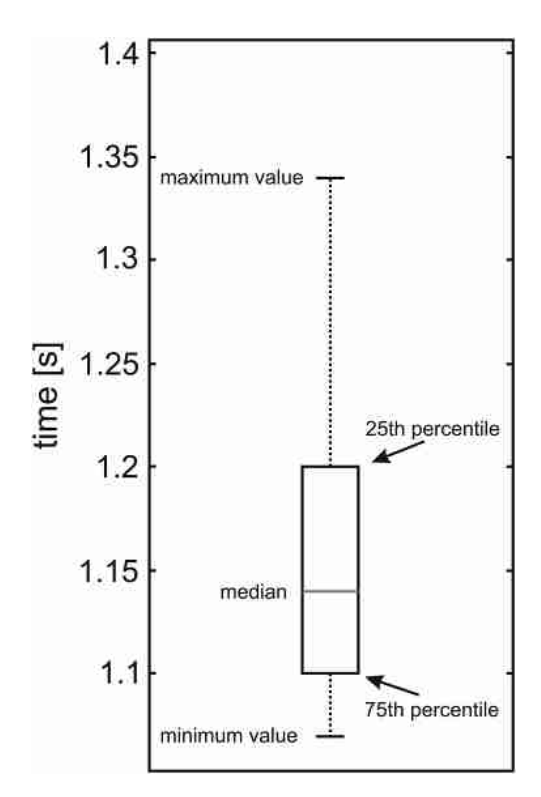


Figure 2. The statistical parameters of the Monte Carlo analysis, median, 25th and 75th percentiles, and the range are displayed for the travel time diagnostic t-50%.

parameters median, 25th and 75th percentiles, and the range are displayed as box-whisker plot for the travel time diagnostic t-50%. With respect to the mathematical derivation of the transformation factor for the inversion of additional travel time diagnostics besides the peak time the reader is referred to *Brauchler et al.* [2003].

2.3. Attenuation Inversion of Pumping Test Data

[22] Brauchler et al. [2011] presented an attenuation integral which relates the attenuation of a Dirac source signal to the inverse of the aquifer parameter specific storage S_s . The line integral reads

$$\left(\frac{h_d(x_2)}{H_{0,d}}\right)^{-\frac{1}{3}} = B^{-\frac{1}{3}} \int_{x_1}^{x_2} \left(\frac{1}{S_s(s)}\right)^{-\frac{1}{3}} ds.$$
 (3)

[23] The attenuation of the Dirac source signal is expressed by the initial displacement H_0 and the hydraulic head $h(x_2)$ at the observation point as a function of the length of the propagation path (s). The subscript d stands for a Dirac source and the parameter B summarizes all test specific parameters that can be treated as constants during the inversion and is defined as follows:

$$B = \frac{\pi r_c^2}{\sqrt{\left(\frac{2\pi}{3}\right)^3}} \exp\left[-\frac{3}{2}\right]. \tag{4}$$

[24] Here r_c is the casing radius of the test well.

[25] The attenuation integral is only valid for a Dirac type source signal. For the determination of the right-hand side of equation (3), the head $h(x_2)$ and H_0 have to be determined. $h(x_2)$ can be easily estimated utilizing the first derivative of the pressure response at the observation interval (Figure 1a). For the determination of the initial displacement H_0 , it is not possible to refer to the first derivative of the pumping signal, because the velocity of the water

movement in the well is largest at t_o , (the point of time when the pumping test is initiated) and this point of time is camouflaged by noise. Hence, we utilize a conversion factor, which allows for relating Heaviside and Dirac signals in order to estimate the initial displacement H_0 . In the following, we summarize the derivation of the conversion factor proposed by *Brauchler et al.* [2003].

2.4. Derivation of the Conversion Factor for a Heaviside Source [After *Brauchler et al.*, 2003]

[26] The solution of the flow equation using a Heaviside source for an infinite domain can be expressed according to *Häfner et al.* [1992] as follows:

$$h_h(r,t) = \frac{Q}{4\pi r K} \operatorname{erfc} \frac{r}{\sqrt{4Kt/S_s}},$$
 (5)

where Q denotes the flow rate, K the hydraulic conductivity and $h_h(r,t)$ is the hydraulic head as function of space and time. Spherical coordinates are used here because each injection port represents a point source and the signal can be assumed to spread radially due to the test intervals. The subscript h stands for a Heaviside source and the maximum drawdown $h_{\rm max}$ is equivalent to $Q/(4\pi rK)$.

[27] The key element of the transformation factor is the introduction of a head ratio α_h , which enables the conversion of a signal originating from a Heaviside source into a signal originating from a Dirac source. α_h is introduced as follows:

$$h_h(r, t_{\alpha,h}) = \alpha_h h_{\text{max}}; \qquad 0 < \alpha_h < 1 \tag{6}$$

[28] Inserting equation (5) in equation (6) yields:

$$\frac{Q}{4\pi rK} \operatorname{erfc} \frac{r}{\sqrt{4Kt_{0.h}/S_{s}}} = \alpha_{h} \frac{Q}{4\pi rK}.$$
 (7)

[29] Utilizing equation (2) to simplify the left-hand side of equation (7) results in:

$$\frac{Q}{4\pi rK}\operatorname{erfc}\sqrt{\frac{3}{2}\frac{t_{\text{peak}}}{t_{\alpha,h}}} = \alpha_h \frac{Q}{4\pi rK}.$$
 (8)

[30] Introducing the conversion factor leads to:

$$\alpha_h = \operatorname{erfc} \sqrt{\frac{3}{2} \frac{t_{\text{peak}}}{t_{\alpha,h}}} = \operatorname{erfc} \sqrt{\frac{3}{2} f_{\alpha,h}}.$$
 (9)

[31] The conversion factor $f_{\alpha,h}$ is 1, if the height of the Heaviside signal is around 8.36% of $h_{\rm max}$. The time and the respective hydraulic head are equivalent to the peak time and the amplitude of a signal with a Dirac source at the origin. By replacing r by r_c in equation (6) this conversion factor can be applied to the signal recorded in the pumping interval if $h_{\rm max}$ is known. In this case $h_{\rm max}$ is defined as drawdown under steady state conditions. In theory, steady state conditions can only be established if a constant head boundary is reached. For an efficient field implementation, we define steady state conditions to be established when the drawdown curve can be approximated by a straight line

with a slope of one tenth of a percent, whereby the slope is defined in meters per second. Figure 1b displays the straight line and $h_{\rm max}$. In conclusion, the amplitude H_0 assuming an impulsive type source is defined by 8.36% of $h_{\rm max}$.

[32] Note, the estimation of $h_{\rm max}$ is an approximation because the derivation of the conversion factor is based on the assumption of a homogeneous hydraulic parameter distribution. However, *Brauchler et al.* [2003] applied this conversion factor successfully to characterize a fractured sand stone sample. In the following, we perform a numerical study based on an aquifer analogue outcrop study in order to show the potential and limits of the proposed hydraulic attenuation inversion.

3. Numerical Example of the Attenuation Inversion Based on an Analogue Outcrop Study

[33] This section builds upon the hydraulic tomography outcrop analogue study performed by Hu et al. [2011]. The outcrop analogue, consisting of fluvial unconsolidated sediments, was developed by Bayer et al. [2011]. The study comprises six parallel high-resolution photographs of an exposed quarry face that were taken every 2 m, as the gravel was excavated. The outcrop photographs were carefully interpreted to yield maps of lithology. For each representative lithological unit, measurements were performed in the laboratory providing porosity, as well as hydraulic conductivity (hydrofacies classification). The specific storage values, assigned to each hydrofacies group were taken from data reported in literature [Domenico and Mifflin, 1965]. Maji and Sudicky [2008] interpolated between the six profiles and translated the gathered information into a 3-D hydraulic parameter distribution. Meanwhile an alternative interpolation based on multiple point statistics is also available [Comunian et al., 2011].

[34] Hu et al. [2011] simulated a suite of short-term pumping tests using a tomographic measurement array, which we will utilize to investigate the possibilities of the attenuation inversion (equations (3)–(9)). The tomographic setup is displayed in Figure 3. For the attenuation inversion, we utilized only source-receiver configurations with a trajectory angle α smaller than 40°. The trajectory angle α is defined as the angle between the horizontal and a straight line connecting source and receiver (Figure 3). Thereby we follow the suggestion of Hu et al. [2011] that data with smaller source-receiver angles are better suited for the reconstruction of horizontally arranged features.

[35] Figure 4 shows the limitations of applying the conversion factor for the processing of data. For source-receiver combinations where the source is located in the high permeability zone between 2.5 and 4 m in vertical position (Figures 4a and 4e), we receive unreasonably high values for the attenuation $h(t)/H_0$. This is not surprising because the derivation of the conversion factor is based on homogeneity assumption, but the aquifer analogue data set is characterized by an up to 5 orders of magnitude range of hydraulic conductivity values (Figures 4a and 4e). For this reason, we neglected source-receiver combinations with a value larger than 0.5 for $h(t)/H_0$. This upper constrain was determined by equation (3). The distance between source (x_1) and receiver (x_2) position was appraised with the well distance. Inserting this parameter in equation (3) gives an

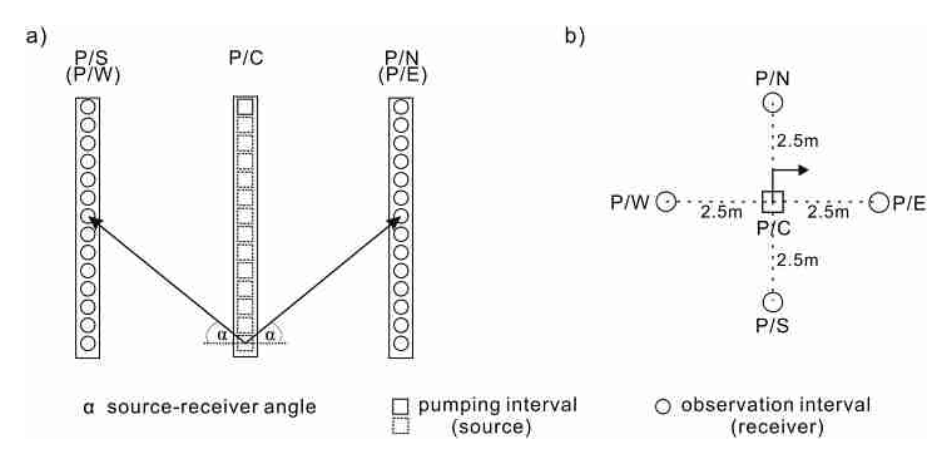


Figure 3. Spatial position of the pumping and observation intervals. (a) Cross section. (b) Plan view.

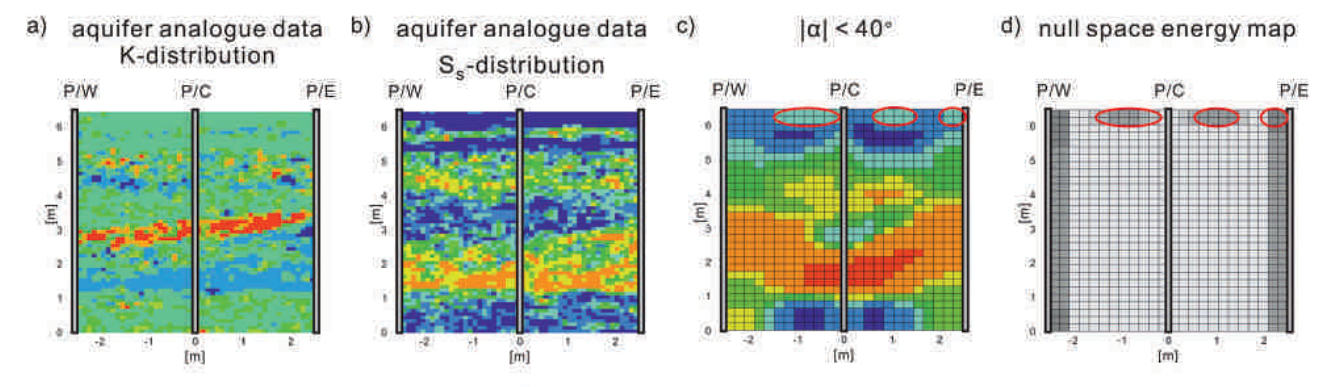
attenuation value of 0.5 that corresponds to a specific storage value of 1.5×10^{-5} 1/m, which represents a lower boundary of specific storage values in fluvial unconsolidated sediments.

[36] The model domain for the inversion consists of eight cells in x-direction (horizontal) and 10 cells in y-direction (vertical). To increase the nominal resolution of the inversion, the staggered grid method is applied [Vesnaver and

Böhm, 2000]. It averages the velocity values obtained from different inversions of a regular coarse gridded model, slightly shifted in space, both in horizontal and vertical directions. We performed such a displacement of the initial grid, three times in *x*- and *y*-direction.

[37] The inversion results for specific storage are displayed in Figures 4c and 4g. Both the reconstructions in West-East and North-South directions show that the most

Aguifer analog data and reconstructed specific storage distributions in West-East-direction:



Aquifer analog data and reconstructed specific storage distributions in South-North-direction:

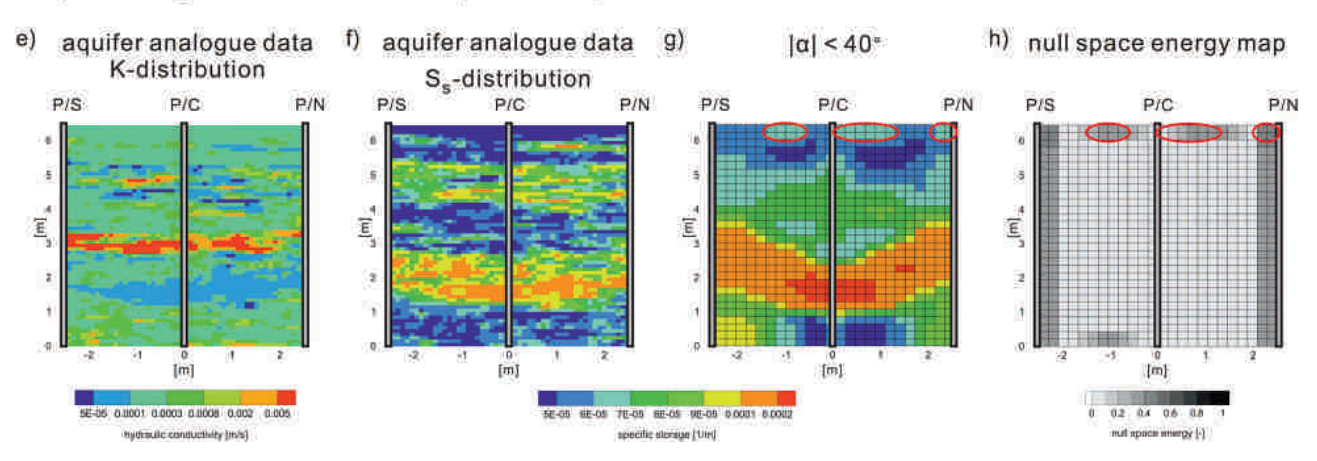


Figure 4. Comparison of the aquifer analog data with the reconstructed specific storage values and the associated null space energy maps. (a–d) Vertical profiles in West-East direction. (e–h) Vertical profiles in South-North direction.

characteristic feature, located between y=1 m and 3 m in vertical direction and characterized by higher specific storage values, could be reconstructed reliably. The horizontal continuity of this zone as well as the absolute values could be determined with adequate precision. The comparison with the true aquifer analogue data set (Figures 4b and 4f) reveals that also the zone between y=4 m and 5 m, characterized by slightly higher specific storage values compared to the background, is reproduced. However, comparison with the aquifer analogue also shows that small-scale variability (< 20 cm in size) using the proposed attenuation inversion procedure cannot be resolved [see also Hu et al., 2011]. In particularly, the zone between y=3 m and 4 m can be reconstructed only close to the test well.

[38] To assess the reliability of the tomographic model we computed the null-space energy map of the area of the model domain. The null-space energy map represents a measure of the reliability of a tomographic system, because it relates the trajectory distribution to the mesh used for the discretization of the investigated area. Further details about the calculation of the null-space energy map are given in Appendix A.

[39] In Figures 4d and 4h, we displayed the null-space energy maps ranging from 0 to 1, whereby a value of 0 indicates a high reliability and a value of 1 a low reliability. In general, the displayed null-space energy maps are characterized by a high reliability, which can be explained with the numerical experimental setup, i.e., high number of test and observation intervals and high-trajectory density, respectively. However, at the boundaries of the model domain the trajectory density is decreasing and thus the reliability is decreasing. The influence of the low reliability can be seen in the reconstructed specific storage tomograms at the top of the model domain, which is characterized by low-specific storage values. Within this zone three positions are marked with red ellipses that are characterized by

higher values. These higher values are associated with a low reliability and, hence, could be potential artifacts.

4. Field Application of the Travel Time and Attenuation Tomography

[40] The field implementation was performed at the well-characterized Stegemühle test site located in the Leine valley, close to Göttingen, Germany. Currently, the infrastructure of the site consists of a network of 26 monitoring locations, comprising 1", 2", 6", screened over the whole aquifer thickness, and multichamber wells (Figure 5). The 6" wells were drilled with a top drive drilling rig, whereas all other wells were installed using DP technology [e.g., Dietrich and Leven, 2006]. Brauchler et al. [2010] give a detailed overview about the structural and hydraulic characterization of the site using conventional investigation techniques. The structural composition of the braided river sediments was characterized by surface refraction seismics, gamma ray logging and DP electrical conductivity logging. For selected wells, cores were recovered to calibrate the recorded logs. The aguifer has a thickness between 2 and 2.5 m, and it is built up by intercalated sand and gravel layers. A confining unit that is composed of silt and clay overlies the aguifer. The thickness of the confining unit varies between 3 and 3.5 m. Figures 6a and 6b show the two DP EC logs recorded at the wells P0/M25 and P5/ M17.5 (Figure 5) that were used as test and observation wells for the field implementation of hydraulic tomography. Hydraulic characterization is based on single-well pumping and cross-well slug interference tests. Hydraulic conductivity estimates, derived from the analytical evaluation of multilevel single-well slug tests, performed over five to seven different depths in each 2" well, vary between 10^{-4} ms⁻¹ and 1.2×10^{-3} ms⁻¹. Generally, the K values increase with aquifer depth (Figure 7).

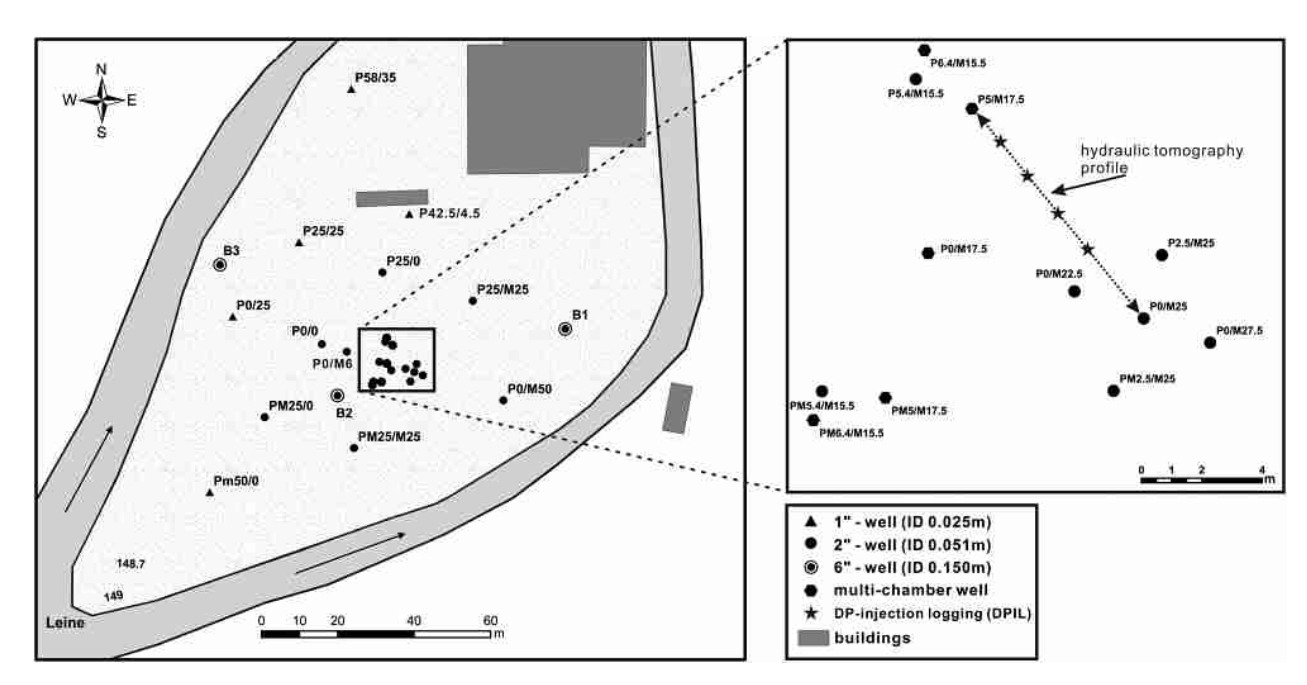


Figure 5. Monitoring well network at the Stegemühle test site.

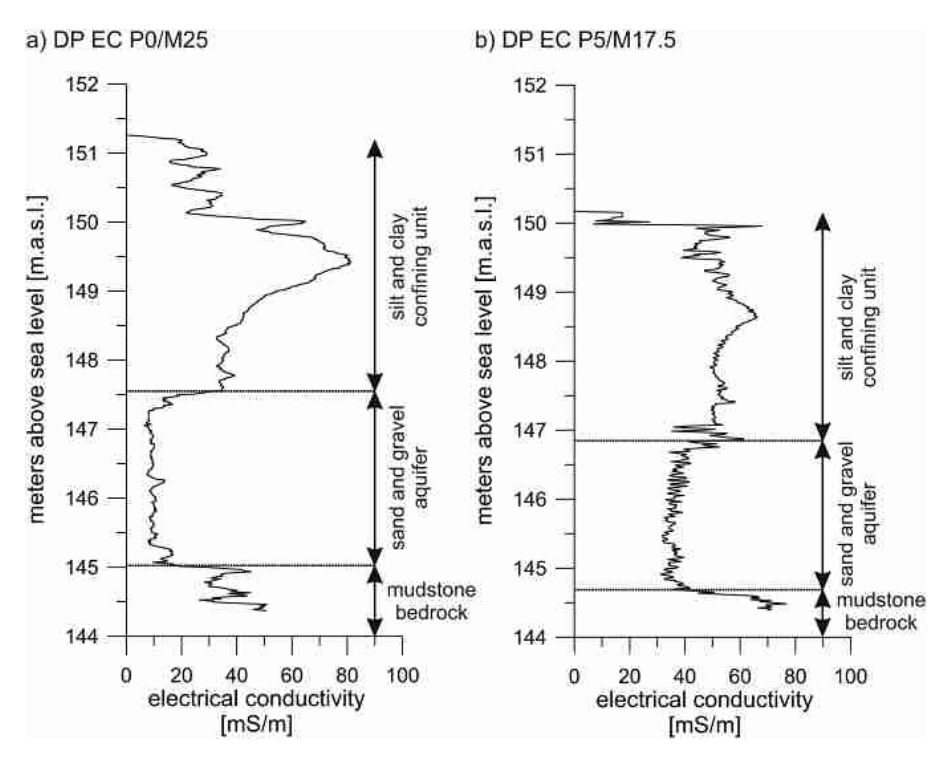


Figure 6. Geological interpretation of the subsurface derived from DP electrical conductivity logging.

[41] The data base for the hydraulic tomographic experiment comprises 30 pressure responses that were recorded between the 2" well (P0/M25) and the multichamber well (P5/M17.5). The experimental setup is displayed in Figure 8. The suite of tomographic pumping tests was recorded by employing a double packer system with a screened interval of 0.25 m and an interval tube inner diameter of 0.031 m in the test well. For the observation well, we utilized the CMT System [Einarson and Cherry, 2002]. This system was originally developed for multilevel sampling and consists of a pipe with seven continuous separate channels or chambers (ID = 0.014 m), which are arranged in a honeycomb shape. In each individual chamber a 0.08 m long opening, covered with a sand filter, was cut. In total five short-term pumping tests were carried out using a double-packer system in the test well, and the respective pressure responses of each test were recorded at six different depth levels in

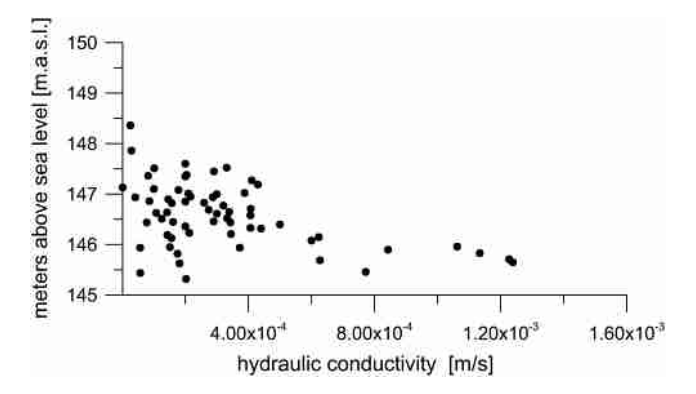


Figure 7. Hydraulic conductivity estimates derived from type curve analysis of multilevel slug tests.

the multichannel well with a frequency of 50 Hz. The experimental setup is displayed in Figure 8

[42] A diffusivity and a specific storage tomogram were reconstructed using the new inversion procedure proposed in section 2. For the diffusivity reconstruction displayed in Figure 9a, the 50% travel time diagnostic was employed for the inversion. The prerequisite of using such an early travel time diagnostic is excellent data quality. Figure 1a clearly shows that it was possible to record pressure drawdown curves with a maximum drawdown below 1 cm with a very low noise level. The model domain consists of 45 cells for both tomograms. Additionally, we applied the method of staggered grid and shifted the mesh four times in

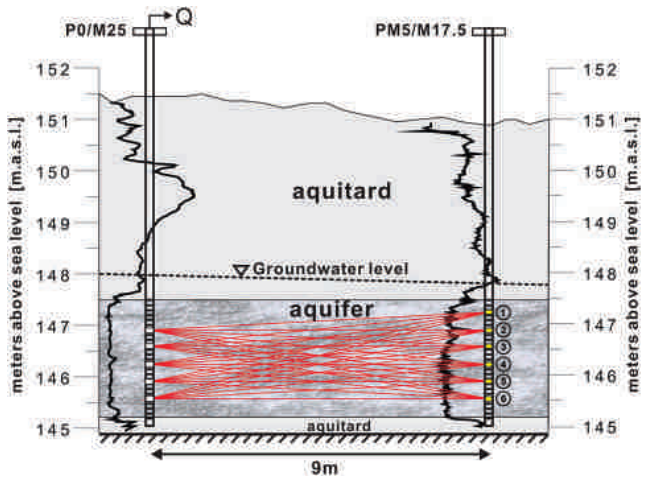


Figure 8. Experimental setup of the hydraulic tomography measurements.

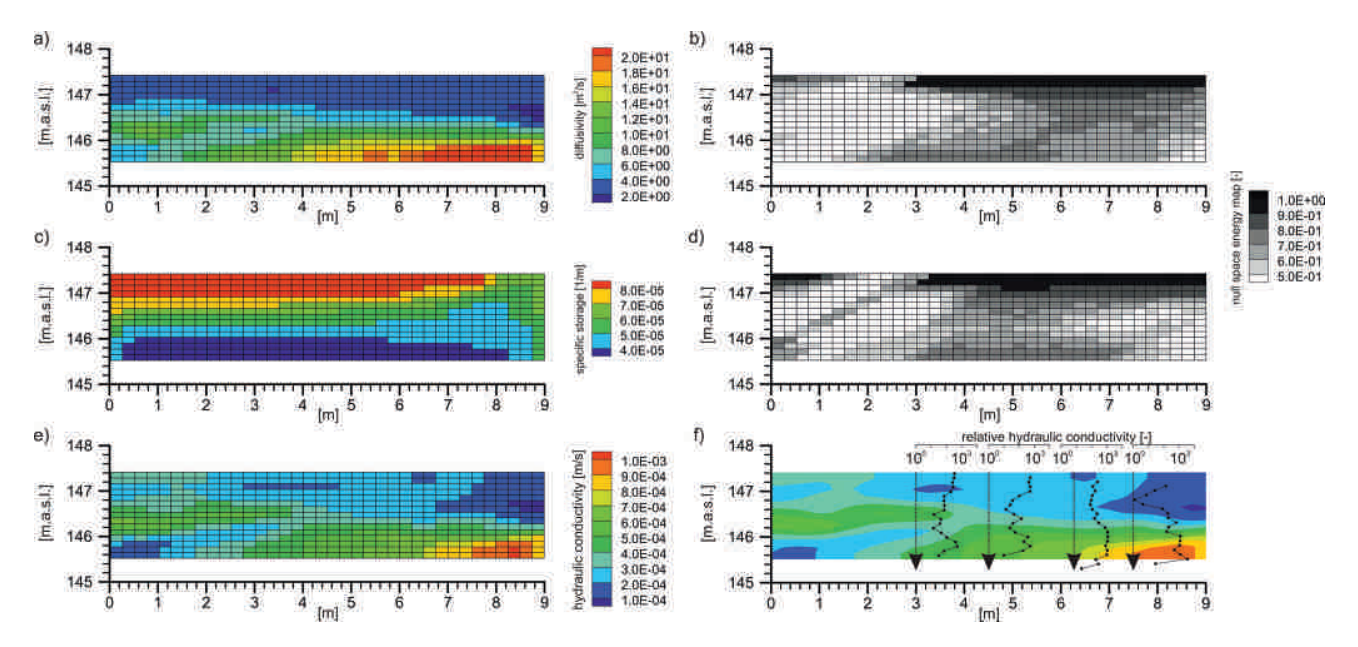


Figure 9. (a, b) Reconstructed diffusivity tomogram and the associated null-space energy map. (c, d) Reconstructed specific storage tomogram and the associated null-space energy map. (e) Computed hydraulic conductivity tomogram utilizing the equation $D = K/S_s$. (f) Comparison of DPIL-logs with an interpolated image of the hydraulic conductivity tomogram.

the horizontal direction and three times in the vertical direction. As starting values we used the parameter estimates derived from the analytical evaluation of the pumping tests data. The travel time and attenuation inversion, including the staggered grid calculation, took less than 1 min on a conventional notebook. For the validation of the tomograms the null space energy maps were calculated (Figures 9b and 9d).

[43] Both diffusivity and specific storage tomograms are characterized by a horizontal layering (Figures 9a and 9c). The reconstructed diffusivity distribution shows the lowest value, approximately 2 m²/s close to aquifer top, and the highest values between 10 and 20 m²/s close to aquifer bottom (Figure 9a). The specific storage distribution is characterized by values between 3×10^{-5} and 10^{-4} 1/m, whereby the lowest values are close to aquifer bottom and the highest ones close to the top (Figure 9c). The hydraulic conductivity tomogram, depicted in Figure 9e, is computed from the equation $D = K/S_s$ and shows a similar parameter distribution as the diffusivity tomogram. The estimated values range from 10^{-4} to 10^{-3} m/s and are representative for sand and gravel aquifers. Furthermore, the range, and the general spatial distribution of the derived hydraulic conductivity values, agrees with the values derived from multilevel slug testing (Figure 7).

[44] The calculated null-space energy maps associated with the diffusivity and specific storage tomogram show both a similar pattern (Figures 9b and 9d). The maps show the highest values (close to 1) indicating a low reliability, at the top of the aquifer between x=3 m and 9 m. in a depth between 147.4 and 147.0 m.a.s.l. The low reliability of these sections can be explained with a low-trajectory density, and the low-trajectory density is caused again by the observation position, which is located 0.2 m below the top of the model domain. Note, the applied inversion technique allows only for the determination of the parameter

space between test and observation interval. The only way to improve the significance of this part is to install a further observation interval at the top of the aquifer.

5. DP Injection Logging

[45] DPIL is a small diameter tool that consists of a short screen located just behind a drive point, which is attached to the lower end of a pipe string [Dietrich et al., 2008]. The probe is advanced in the ground by using the weight of the DP unit supported by a hydraulic jack hammer. During advancement in the ground, water is injected through the screen in order to avoid clogging. As soon as the desired test depth is reached, further advancement is stopped and a series of tests are performed. In this field study, at the Stegemühle site, testing was performed with three different injection (flow) rates. Flow rate and pressure were measured on-site. Both can be transformed into a relative hydraulic conductivity estimate $K_{\rm DPIL}$, which can be used as a proxy for K. For details on the derivation of $K_{\rm DPIL}$ the reader is referred to Dietrich et al. [2008].

[46] We recorded five profiles, each comprising between 15 and 20 measurement intervals. The profiles were recorded between the test and observation well used for the short-term pumping tests (Figure 5). However, only four profiles could be evaluated because one log exhibited a strong dependence between flow rate and $K_{\rm DPIL}$, which indicates technical problems with the flow controller or trunk line. In Figure 9e, the profiles are displayed in comparison to the reconstructed hydraulic conductivity tomogram.

[47] The comparison between the DPIL profiles with the reconstructed hydraulic conductivity tomogram shows an overall agreement that the highest hydraulic conductivity values are below 146 m.a.s.l. That means the top of the higher permeability zone can be determined in the DPIL logs as well as in the hydraulic conductivity tomogram.

Beyond this, the DPIL logs recorded at x-directions 6.2 m and 7.5 m agree over the whole thickness of the aquifer. In particular, the agreement between the DPIL log recorded at the position x=7.5 m, characterized by the lowest $K_{\rm DPIL}$ in a depth 146.8 m.a.s.l. and highest $K_{\rm DPIL}$ values of all logs in a depth of 146.2 m.a.s.l agrees in all details with the reconstructed hydraulic conductivity tomogram. Note, the positions of the DPIL profiles are shown by the black arrow in Figure 9f.

[48] The upper part of the DPIL logs, above 147 m.a.s.l., at x-directions 3 m and 4.5 m indicates changes in hydraulic conductivity not reconstructed in the hydraulic conductivity tomograms. One explanation for the lack of dynamics in the hydraulic conductivity tomogram could be the different resolution of the two characterization techniques. The DPIL logs display the hydraulic properties in the vicinity of the open screen section. That means small-scale heterogeneities on the sub decimeter scale strongly influences the DPIL results. However, the numerical example has shown that the applied tomographic inversion scheme is not able to resolve such small scale heterogeneities. Another explanation could be the low reliability of the hydraulic conductivity tomogram above 147 m.a.s.l. indicated by the calculated null-space energy maps (Figures 9b and 9d). The decline of the K_{DPIL} values below 146.4 m.a.s.l can be explained by the transition from the aquifer to the underlying aquitard. This transition zone is interpreted as a mix of aquifer material and weathered marl stone. Note this zone could not be reconstructed by the hydraulic tomography, because all source and receiver positions were located within the aquifer. Still, the agreement of the DPIL profiles and the reconstructed K-tomogram supports the reliability of the estimated spatial distribution of the hydraulic properties estimated with the travel time and attenuation tomography, as well as with the DPIL.

6. Conclusions

[49] We presented a field assessment of high-resolution aquifer characterization of unconsolidated sediments based on hydraulic tomography and DP injection logging. The results show that both, the hydraulic tomograms and the DP injection logging provide information about hydraulic subsurface parameters with a spatial resolution that would not be feasible with conventional hydraulic investigation and evaluation technologies. However, for practical implementation, the following aspects have to be considered: (1) equipment requirements, (2) time demand for field implementation, (3) complexity or easiness of the evaluation.

[50] (1) The equipment requirements for both methods are comparable: Both methods require a DP unit in order to access the subsurface i.e., for probe advancement and well installation. Beyond this standard pumping test equipment, a double-packer system is needed to record a suite of hydraulic tomography measurements. For the hydraulic profiling the DP injection logger consisting of a screened metal cone, trunk-line, flow controller and pressure transducer, is needed. We think in comparison to conventional hydraulic field testing, which relies on existing wells, the requirements for both investigation technologies can be justified with respect to the gained spatial high resolution parameter estimates.

- [51] (2) The DPIL, as well as the short-term pumping test, can be performed in one day including test setup. In this field study, we pumped for 5 min, which is more than sufficient for the applied travel time and attenuation based inversion scheme. Short pumping time can be a limitation for other inversion schemes that are based on solving the groundwater flow equation, because the early times are mainly determined by the specific storage, S_s , distribution, and later times or even steady state conditions are better suited for reconstructing the K-field [$Wu\ et\ al.$, 2005; R. Sun, et al., A temporal sampling strategy for transient hydraulic tomography analysis, submitted to $Water\ Resources\ Research$, 2012].
- [52] For the hydraulic tomography measurements, an additional day is needed for well installation. However, an experienced field technician team can install five DP wells with a depth of 10 m easily in 1 day. Note, by installing a larger number of observation wells more than one tomographic profile can be recorded without substantially increasing the workload.
- [53] (3) We adapted the travel time and attenuation based inverse scheme proposed by Brauchler et al. [2011] to the requirements needed for the tomographic inversion of short-term pumping tests in order to minimize the complexity and time requirements for hydraulic tomography inversion. The main advantages of the inversion scheme are the low computational requirements of eikonal solvers and that no information about the hydraulic boundary conditions of the investigated area is needed. However, the applied inversion scheme can only reconstruct the parameter reconstruction between test and observation well. The processing of the short-term pumping test data can be largely automatized using any script language, and for the inversion user-friendly eikonal solvers are commercially available. The short pumping time in combination with the straightforward inversion technique allows for the reconstruction of preliminary K and S_s distribution already in the field, which is particularly useful for an adaptive site investigation approach. In this context, it has also to mention that inversion schemes that solve the groundwater flow equation might reconstruct hydraulic conductivity fields that are closer to the true parameter distribution. However, as mentioned above short-term pumping test are not well suited for these inversion approaches because fitting later times of a transient pressure curve or even steady state conditions lead to better *K*-field reconstructions.
- [54] The evaluation of the DPIL is based on a simple spread sheet calculation and the relative $K_{\rm DPIL}$ values can be estimated directly in the field. The shortcomings of the DPIL providing relative $K_{\rm DPIL}$ values can be overcome by using complementary measurements such as DP slug tests or by using other probes such as the high resolution K profiling tool (HRK).
- [55] The field assessment of the new hydraulic tomography framework and comparison with DPIL showed that both methods provide information about hydraulic conductivity on a scale and accuracy which goes beyond the expressiveness of conventional hydraulic testing. The further developed hydraulic attenuation inversion scheme additionally allows for the reconstruction of specific storage distribution. At the Stegemühle site it was revealed that a spatially high resolution of the parameter estimates derived from hydraulic

tomography can be recorded and evaluated in a short amount of time, which even allows for an adaptive site characterization, i.e. deciding immediately on-site about measurements to be performed next, based on prior investigation results. Beyond this, hydraulic parameter estimates with such a spatially high resolution have the potential to strongly increase the significance of hydrogeophysical investigations [Brauchler et al., 2012].

Appendix A

[56] In the following, we give a short summary of the calculation of the of the null-space energy map, which is based on the work of $B\ddot{o}hm$ and Vesnaver [1996]. The null space energy map was originally developed for the validation of geophysical ray tomograms. The null space energy map comprises a singular value decomposition of the tomographic matrix $\bf A$, where A_{ij} of the matrix $\bf A$ are the lengths of the ith trajectory path in the jth cell. This matrix can be factorized into three components:

$$\mathbf{A} = \mathbf{U}\mathbf{W}\mathbf{V}^{\mathsf{T}} \tag{A1}$$

[57] The squared matrices U and V are orthonormal:

$$\mathbf{U}\mathbf{U}^{\mathbf{T}} = \mathbf{I}, \quad \mathbf{V}\mathbf{V}^{\mathbf{T}} = \mathbf{I} \tag{A2}$$

[58] **U** and the elements w_{ii} of the diagonal matrix **W** are the singular values corresponding to the square of the eigenvalues. The stability of the tomographic inversion is defined by the elements w_{ii} , whereby small singular values show instabilities of the inversion process. Note, the columns of the matrix **V** of the decomposition (equation (A1)) display an orthonormal basis of the model domain. Hence, the local reliability, R, of each pixel can be defined as the summation of the squared elements v_i of the matrix **V**:

$$R = \sum_{i} v_i^2. \tag{A3}$$

- [59] The summation of the elements is equal to 1 if the index i covers the whole model domain and each pixel is associated with a value ranging from 0 to 1.
- [60] Acknowledgments. The investigations were conducted with the financial support of the Swiss National Science Foundation to the project "A field assessment of high-resolution aquifer characterization: An integrated approach combining hydraulic tomography and tracer tomography" under grant number 200021_140450/1 and the financial support of the German Research Foundation to the project "High resolution aquifer characterization based on direct-push technology: An integrated approach coupling hydraulic and seismic tomography" under grant no. BR3379/1-2. We would like to thank Gualtiero Böhm for his help with the null space energy maps. This manuscript greatly benefited from comments by Jungfeng Zhu and two anonymous reviewers.

References

- Bayer, P., P. Huggenberger, R. Renard, and A. Comunian (2011), Three-dimensional high resolution fluvio-glacial aquifer analog, Part 1: field study, *J. Hydrol.*, 405, 10–23.
- Berg, S. J., and W. A. Illman (2011), Three-dimensional transient hydraulic tomography in a highly heterogeneous glaciofluvial aquifer-aquitard system, *Water Resour. Res.*, 47, W10507, doi:10.1029/2011WR010616.
- Böhm, G., and Vesnaver, A. (1996), Relying on a grid, *J. Seismic Explor.*, 5, 169–184.

- Bohling, G. C., X. Zhan, J. J. Butler Jr., and L. Zheng (2002), Steady shape analysis of tomographic pumping tests for characterization of aquifer heterogeneous, *Water Resour. Res.*, 38(12), 1324, doi:10.1029/2001WR001176.
- Bohling, G. C., J. J. Butler, Jr., X. Zhan, and M. D. Knoll (2007), A field assessment of the value of steady-shape hydraulic tomography for characterization of aquifer heterogeneities, *Water Resour. Res.*, 43, W05430, doi:10.1029/2006WR004932.
- Bohling, G. C., G. Liu, S. Knobbe, E. Reboulet, D. W. Hyndman, P. Dietrich, and J. J. Butler Jr. (2012), Geostatistical analysis of centimeter-scale hydraulic conductivity variations at the MADE site, *Water Resour. Res.*, 48, W02525, doi:10.1029/2011WR010791.
- Boggs, J. M., S. C. Young, and L. M. Beard (1992), Field study of dispersion in a heterogeneous aquifer, 1, Overview and site description, *Water Resour. Res.*, 28(12), 3281–3291.
- Brauchler, R., R. Liedl, and P. Dietrich (2003), A travel time based hydraulic tomographic approach, *Water Resour. Res.*, 39(12), 1370, doi:10.1029/2003WR002262.
- Brauchler, R., J.-T. Cheng, M. Everett, B. Johnson, P. Dietrich, R. Liedl, and M. Sauter (2007), An inversion strategy for hydraulic tomography: Coupling travel time and amplitude inversion, *J. Hydrol.*, 345, 184–198, doi:10.1016/j.jhydrol.2007.08.011.
- Brauchler, R., R. Hu, T. Vogt, D. Halbouni, T. Heinrichs, T. Ptak, and M. Sauter (2010), Cross-well interference slug tests: An efficient tool for high resolution characterization of hydraulic heterogeneity, *J. Hydrol.*, 384, 33–45, doi:10.1016/j.jhydrol.2010.01.004.
- Brauchler, R., R. Hu, P. Dietrich, and M. Sauter (2011), A field assessment of high-resolution aquifer characterization based on hydraulic travel time and hydraulic attenuation tomography, *Water Resour. Res.*, 47, W03503, doi:10.1029/2010WR009635.
- Brauchler, R., J. Doetsch, P. Dietrich, and M. Sauter (2012), Derivation of site-specific relationships between hydraulic parameters and p-wave velocities based on hydraulic and seismic tomography, *Water Resour. Res.*, 48, W03531, doi:10.1029/2011WR010868.
- Butler, J. J., Jr. (2005), Hydrogeological methods for estimation of hydraulic conductivity, in *Hydrogeophysics*, edited by Y. Rubin and S. Hubbard, pp. 23–58, Springer, Dordrecht.
- Cardiff, M., W. Barrash, P. K. Kitanidis, B. Malama, A. Revil, S. Straface, and E. Rizzo (2009), A potential-based inversion of unconfined steady-state hydraulic tomography, *Ground Water*, 47(2), 259–270, doi:10.1111/j.1745-6584.2008.00541.x.
- Cheng, J.-T., R. Brauchler, and M. E. Everett (2009), Comparison of early and late travel times of pressure pulses induced by multilevel slug tests, *Eng. Appl. Comput. Fluid Mech.*, 3 (4), 514–529.
- Comunian, A., Renard, P., Straubhaar, J., and P. Bayer (2011), Three-dimensional high resolution fluvio-glacial aquifer analog, Part 2: geo-statistical modelling, *J. Hydrol.*, 405, 10–23.
- Dietrich, P., J. J., Butler, Jr., and K. Faiß (2008), A rapid method for hydraulic profiling in unconsolidated formations, *Ground Water*, 46(2), 323–328
- Dietrich, P., and C. Leven (2006), Direct push technologies, in *Groundwater Geophysics*, edited by R. Kirsch, pp. 321–340, Springer, Berlin.
- Domenico, P. A., and M. D. Mifflin (1965), Water from low-permeability sediments and land subsidence, *Water Resour. Res.*, 1(4), 563–576.
- Einarson, M. D., and J. A. Cherry (2002), A new multilevel ground water monitoring system using multichannel tubing, *Ground Water Monit.* Rem., 22(4), 52–65.
- Häfner F., D. Sames, and H.-D. Voigt (1992), Wärme und Stofftransport Mathematische Methoden, 626 pp., Springer, Berlin.
- Hu, R., R. Brauchler, M. Herold, and P. Bayer (2011), Hydraulic tomography analog outcrop study: Combining travel time and steady shape inversion, *J. Hydrol.*, 409(1-2), 350–362, doi:10.1016/j.jhydrol.2011.08.031.
- He, Z., A. Datta-Gupta, and D. W. Vasco (2006), Rapid inverse modeling of pressure interference tests using trajectory based traveltime and amplitude sensitivities, *Water Resour. Res.*, 42, W03419, doi:10.1029/2004 WR003783.
- Huang, S.-Y., J.-C. Wen, T.-C. J. Yeh, W. Lu, H.-L. Juan, C.-M., Tseng, J.-H. Lee, and K.-C. Chang (2011), Robustness of joint interpretation of sequential pumping tests: Numerical and field experiments, *Water Resour. Res.*, 47, W10530, doi:10.1029/2011WR010698.
- Illman, W. A., X. Liu, S. Takeuchi, T.-C. J. Yeh, K. Ando, and H. Saegusa (2009), Hydraulic tomography in fractured granite: Mizunami Underground Research site, *Jpn. Water Resour. Res.*, 45, W01406, doi:10.1029/ 2007WR006715.
- Kitanidis, P. K. (1995), Quasi-linear geostatistical theory for inversing, Water Resour. Res., 31(10), 2411–2419.

BRAUCHLER ET AL.: RAPID FIELD APPLICATION OF HYDRAULIC TOMOGRAPHY

- Li, W., A. Englert, O. A. Cirpka, and H. Vereecken (2008), Three-dimensional geostatistical inversion of flowmeter and pumping test data, Ground Water, 46(2), 193–201.
- Liu, G., J. J. Butler Jr., G. C. Bohling, E. Reboulet, S. Knobbe, and D. W. Hyndman (2009), A new method for high-resolution characterization of hydraulic conductivity, *Water Resour. Res.*, 45, W08202, doi:10.1029/2009WR008319
- Liu, G., J. J., Butler, Jr., E. Reboulet, and S. Knobbe (2012), Hydraulic conductivity profiling with direct push methods, *Grundwasser*, 17(1), 19–29, doi:10.1007/s00767-011-0182-9.
- Maji, R., and E. A. Sudicky (2008), Influence of mass transfer characteristics for DNAPL source depletion and contaminant flux in a highly characterized glaciofluvial aquifer, *J. Contam. Hydrol.*, 102(1-2), 105–119.
- McCall, W., T. M. Christy, T. Christopherson, and H. Isaacs (2009), Application of direct push methods to investigate uranium distribution in an alluvial aquifer, *Ground Water Monit. Rem.*, 29(4), 65–76.
- Paige, C. C., and M. A. Saunders (1982), LSQR: An algorithm for sparse linear equations and sparse least squares, *ACM Trans. Math. Software*, 8(1), 43–71, doi:10.1145/355984.355989.
- Rehfeldt, K. R., J. M. Boggs, and L. W. Gelhar (1992), Field study of dispersion in a heterogeneous aquifer, 3, Geostatistical analysis of hydraulic conductivity, *Water Resour. Res.*, 28(12), 3309–3324.
- Straface, S., T.-C. J. Yeh, J. Zhu, S. Troisi, and C. H. Lee (2007), Sequential aquifer tests at a well field, Montalto Uffugo Scalo, Italy, *Water Resour. Res.*, 43, W07432, doi:10.1029/2006WR005287.

- Vasco, D. W., H. Keers, and K. Karasaki (2000). Estimation of reservoir properties using transient pressure data: An asymptotic approach, *Water Resour. Res.*, 36(9), 3447–3465.
- Vesnaver, A., and G. Böhm (2000), Staggered or adapted grids for seismic tomography, *Leading Edge*, 19(9), 944–950.
- Virieux, J., C. Flores-Luna, and D. Gibert (1994) Asymptotic theory for diffusive electromagnetic imaging, *Geophys. J. Int.*, 119, 857– 868.
- Wenzel, L. K. (1942), Methods for determining permeability of water-bearing materials, with special reference to discharging-well methods, U.S. Geol. Surv. Water Supply Pap., 887, 192.
- Wu, C.-M., T.-C. J. Yeh, J. Zhu, T. H. Lee, N.-S. Hsu, C.-H. Chen, and A. F. Sancho (2005), Traditional analysis of aquifer tests: Comparing apples to oranges? *Water Resour. Res.*, 41, W09402, doi:10.1029/ 2004WR003717.
- Xiang, J., T.-C. J. Yeh, C.-H. Lee, K.-C. Hsu, and J.-C. Wen (2009), A simultaneous successive linear estimator and a guide for hydraulic tomography analysis, *Water Resour. Res.*, 45, W02432, doi:10.1029/2008WR007180.
- Yaramanci, U., G. Lange, and M. Hertrich (2002), Aquifer characterization with surface-NMR and other geophysical techniques at the test site Nauen/Berlin, *J. Appl. Geophys.*, 50(1–2), 47–65.
- Zhu, J., and T.-C. J. Yeh (2005), Characterization of aquifer heterogeneity using transient hydraulic tomography, *Water Resour. Res.*, 41, W07028, doi:10.1029/2004WR003790.